ISSN 1070-4272, Russian Journal of Applied Chemistry, 2024, Vol. 97, No. 1, pp. 88–103. © Pleiades Publishing, Ltd., 2024.

MEMBRANES

Polyethersulfone/Chamomile Mixed Matrix Membrane for Methylene Blue Dye Removal from Wastewater

Rana I. Raja[a,*], Khalid T. Rashid[a,], and Manal A. Toma[a,***]**

[a] *Membrane Technology Research Unit, Chemical Engineering Department, University of Technology-Iraq, Baghdad, 10066 Iraq*
**e-mail: che.21.16@grad.uotechnology.edu.iq*
***e-mail: Khalid.T.Rashid@uotechnology.edu.iq*
****e-mail: manal.a.toma@uotechnology.edu.iq*

Received March 11, 2024; revised March 17, 2024; accepted April 2, 2024

Abstract—Flux decline is one of the most significant defies ultrafiltration (UF) must overcome. One viable approach to address this issue involves the implementation of nano-additives into the membrane matrix. In this research, the potential of chamomile leaf nanoparticles (Chm NPs) as an eco-friendly material for use in UF membrane synthesis was explored. To better understand the impact of Chm on the production of PES UF membranes, a range of membranes were created by introducing varying amounts of Chm into the casting solution. The produced membranes were thoroughly evaluated, focusing on aspects such as porosity, pore size, hydrophilicity, membrane morphology, and UF performance. Manufactured PES/Chm membranes demonstrated significantly increased permeate water flux (PWF) (up to 367 L/m^2 h), which was three times that of the pristine PES membrane (126 L/m^2 h). Beside Methylene Blue dye (MB) rejection, it was obtained a high removal percent of about 94 %. Additionally, decreased contact angle (C.A.) for modified membranes (47%), compared with pristine PES membranes, all these results led to enhance the membrane permeate flux and rejection. The utilization of chamomile as a novel environmentally friendly addition holds significant potential in the production of UF membranes for wastewater treatment.

Keywords: ultrafiltration (UF), Methylene Blue dye, eco-friendly material, chamomile; AG, arabic gum

DOI: 10.1134/S1070427224010130

ABBREVIATIONS AND NOTATION

TE—thyme extracts;
CS—Chitosan;
BSA—Bovine serum albumin;
PES—Polyethersulfone.

INTRODUCTION

Improvements in processing speed and decreases in energy usage have resulted from significant growth in the chemical industries during the previous few decades. The overall processing cost is significantly impacted by the separation and purification of various components, which is acknowledged as a crucial approach in chemical and biochemical engineering. Fresh water shortage increases the risk of conflict, public health problems, reduction in food production, inhibition of industrial product expansion, and these problems threaten the environment. The discharge of inadequately treated industrial waste water can therefore have far-reaching consequences; physical effects, toxic effects on aquatic life, eutrophication. Therefore, while various purifying methods such as flocculation, adsorption, and distillation have been designed and developed, they often necessitate intricate equipment, high energy use, and significant operation costs. Membrane separation technology, however, has garnered interest due to its high selectivity, relatively low energy usage, and minimal chemical reliance [1, 2]. The incorporation of beneficial characteristics from the polymer matrix and active elements of additives provide these enhanced membranes with numerous advantages. Additionally, the

employment of these environmentally friendly additives holds a positive impact on the environment [1, 3, 4]. The use of environmentally friendly additives, green solvents or natural additives all present viable strategies to achieve goals related to membrane modifications. Research has been conducted on natural additives like Gum Arabic, chitosan, and clay minerals, leading to the belief that these natural substances may serve as beneficial hydrophilic enhancements to membrane matrices. These naturally derived components have been the subject of numerous recent studies [5, 6].

To address the challenges posed by the discharge of hazardous biocidal agents, Ahmadi et al. [7] were able to synthesize two novel chitosan-based membranes were synthesized via surface modification of polyethersulfone (PES) membranes incorporating garlic and thyme as herbal antibacterial extracts. The findings suggested a significant antibacterial capacity. The addition of garlic extract to chitosan solution resulted in a significant increase in the discharge of purified water through the GE-CS/PES membrane (85.22 L/m^2 h). The addition of herbal extract to the surface of the membrane resulted in a significant improvement in the removal of chemical oxygen demand (COD). In contrast, the TE-CS/PES membrane demonstrated the highest rejection ability at 98.71%. Modified membrane achieved the maximum flux recovery ratio (90.56%) and an improvement in antifouling capability. Saja, et al. [8] describes the fabrication and characterization of a ceramic perlite-supported ultrafiltration bentonite membrane at a minimal cost. It was proven that the improved membrane made with 0.75 wt % bentonite is uniform and sticks well to the perlite support. In addition, the membrane is 6 μm thick, has pores that are 13 nm wide, and lets 30 L/(h m^2 bar) through. Furthermore, the filtration efficiency of the bentonite membrane was assessed through tangential filtration of solutions containing Rhodamine B and Direct Red 80 at a pressure of 4 bar. An investigation into the influence of filtration time and initial feed concentration on flux and rejection revealed that Direct Red 80 and Rhodamine B rejection values could reach 97.0 and 80.1%, respectively. Through the use of the phase inversion approach, Manawi et al. [9] were able to successfully blend a polysulfone membranes with Arabic gum, which may be used as a pore-forming agent. The study investigated the performance of freshly synthesized PS/AG membranes that were cast in dope solutions with varying concentrations of AG ranging from 0.1 to 3.0 wt %. During BSA solution filtration, membranes were tested for antifouling and antibacterial characteristics using *Escherichia coli*.

Chai et al. [10] assembled a hydrophilic mixed matrix membrane (MMM) by utilizing the polysulfone (PSf) polymer, graphene oxide (GO) nanomaterial, and the environmentally friendly substance gum Arabic (GA). According to the outcome of the characterization study, the MMM designed with 0.6 wt % of GO exhibited the highest porosity, the largest average pore size, and enhanced hydrophilicity due to the oxygen-containing functional groups associated with GO and GA. These factors contributed to the highest water flux result. Concurrently, the membrane displayed a superb rejection property and improved antifouling capability, along with a notable rejection of humic acid. This summed up to its already admirable antifouling ability. To maximize the ultrafiltration membranes' performance, pre-use modifications are required. Enhancing the membranes' hydrophilicity is seen as a viable approach to boost their performance. In fact, these modification techniques strike a balance between the hydrophilic and hydrophobic characteristics of polymeric membranes, enhancing the separation properties, which in turn improve the removal of ions and organic molecules from aqueous solutions [11].

This study examined the impact of incorporating Chamomile powder into the casting solution of a PES membrane. Due to the fact that it is compatible with PES and has favorable characteristics, chamomile powder was selected for use as a hydrophilic green addition in the current investigation. Through the incorporation of chamomile powder into the membrane casting solution, it is anticipated that the hydrophilicity of the membrane would be enhanced. This is due to the fact that chamomile forms a hydroxyl group bond on the PES membrane surface, with the different concentration of chamomile in the membrane matrix will vary greatly. The impact of Chm NPs on the permeability characteristics, structure, and hydrophilicity of the membrane were thoroughly explored and well described. A cross-sectional and top surface examination of the morphology of each membrane was conducted utilizing Field Emission Scanning Electron Microscopy (FESEM). Water permeability, CR, MB dyes, and bovine serum albumin (BSA) rejection at varying feed quantities were used to evaluate the membranes' capabilities.

Table 1. Composition of pure and blended PES membranes (wt %)

Membrane	PES	Chm NPs	NMP
RM_0	16	0	84
$RM_{Chm0.5}$	16	0.5	83.5
RM_{Chm1}	16	1	83
$RM_{Chm1.5}$	16	1.5	82.5
RM_{Chm2}	16	2	82

EXPERIMENTAL

Materials. The base polymer for membrane manufacture is polyethersulfone (PES) with a molecular weight of 30 000 g/mol, which was obtained from Solvay Advanced Polymers in Belgium. N-Methyl-2-pyrrolidone (NMP, C_5H_9NO with 99% purity) as a solvent was acquired from Thomas Baker, chamomile leaves were obtained from local markets as additives, and methylene blue (MW = of 319.85 g/mol) was obtained from HIMEDIA-India Company.

Preparation of green additives. The green additives (chamomile leaves) are cleaned in clean water to remove any remaining dust and other impurities, and then they are dried in a hot air oven at 35°C for an hour to make sure there is no moisture left. To get rid of impurities and unwanted parts, such as coarse particles, the best method is to sift using a fine sieve. The final step involves 20 h of mechanical grinding to produce smooth particles, or nanoparticles.

PES/Chm membrane preparation. Asymmetric flat sheet polyethersulfone (PES) membranes were manufactured through immersion precipitation, which initiated the phase inversion process [12].To ascertain the Chm content in the PES membrane solution, a specific amount of Chm was mixed with the N-Methyl-2-pyrrolidone (NMP, C_5H_9NO) solvent, ensuring a steady mix at a consistent temperature, as represented in Table 1. The final blend was stowed in a side drier overnight at a preservation-friendly temperature, not exceeding 40°C. Before the casting process, the casting solution was subjected to ultra-sonication for one hour. Then, a determined amount of casting solution was layered on a flat glass panel and spread out with a casting knife (A.F.A.-IV; China), adjusting the air gap to 200 μm. To remove the solvent and set the resulting thin film, the glass panel was instantly immersed in a coagulation bath of distilled water at room temperature. Lastly, the resulting nanocomposite membrane was rinsed with deionized water and kept for further analysis (Fig. 1).

Characterization of chamomile nanoparticles. The mean particle size of Chm NPs was measured using Dynamic Light Scattering (DLS) (provided

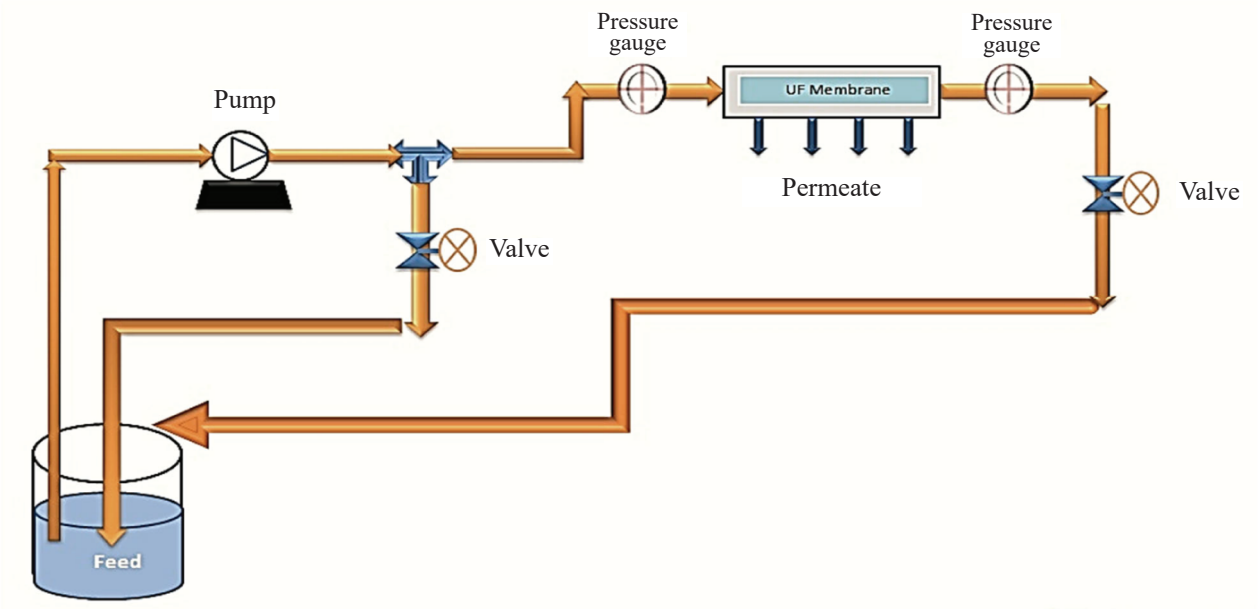

Fig. 1. Schematic diagram of a UF-unit operating in cross-flow mode.

by Brookhaven Inst. Corp., USA). The dried Chm particles' chemical composition was examined using a FTIR spectrometer (IRAffinity-1, SHIMADZU, Japan). Each ATR-FTIR spectrum was gathered with a 4 cm^{-1} resolution, ranging from 800 to 2000 cm^{-1}.

MEMBRANE CHARACTERIZATION

Contact angle measurement. For hydrophilicity measurements, an optical instrument (110-O4W CAM, Taiwan) was employed to detect the water contact angle of the samples. In this method, a 3 μL of a deionized water droplet at room temperature was placed onto the membrane surface using a microliter syringe. The profile of the water droplet on the surface was captured by an optical subsystem with a digital camera. The average value of each membrane was calculated at five locations for each sample.

Porosity and pore size estimation. Porosity (ε) and pore size (r_m) analysis for the fabricated membranes were determined via gravimetric method as defined by Eq. (1) and Guerout–Elford–Ferry equation [Eq. (2)], respectively [13]:

$$\varepsilon = \frac{\omega_1 - \omega_2}{Al\rho}, \quad (1)$$

$$r_m = \sqrt{\frac{(2.9 - 1.75\varepsilon)8\eta lQ}{\varepsilon A \Delta P}}, \quad (2)$$

where ω_1 and ω_2 are the weights of the wet and dry membranes, A is the membrane area (cm^2), l is the membrane thickness (cm), and represents the density of pure water (g cm^{-3}). To reduce experimental error, the final value for each membrane was averaged from three samples, η is the water viscosity (8.9×10^{-4} Pa s), Q is the volume of permeated pure water per unit time (m^3/min), and ΔP is the operating pressure (0.1 MPa).

Membrane thickness. The membrane's thickness has a major impact on the membrane filtration process. The membrane's thickness was measured with an ISO 9001 digital micrometer. Using the SEM approach, the thickness of the created membranes may also be specified. An average of seven measurements taken at different locations on membranes was calculated using a micrometer (range 0–100 mm, precision: 2 μm, HDT, China).

Membrane morphology. FESEM (Inspect F50, ELECMI, Spain) was used to examine the surface and cross-sectional morphology of the fabricated membranes, which provides the visual information on the top surface as well as cross-sectional of the membrane structures. Membranes were cut into small pieces and cleaned with filter paper. Membrane samples immersed in liquid nitrogen for about 1–3 min were broken to examine the cross-sectional morphologies and kept in the air for drying. The dried samples were sputtered with a thin gold thin layer using a rotary-pumped coating system for producing electric conductivity. After sputtering with gold, they were viewed with the microscope.

Membrane performance. Analyzing pore size and membrane porosity is crucial; as they directly impact the membrane's rejection ability and permeation flux, respectively. Typically, the porosity of a membrane is tied to the mass transfer rate between the solvent and non-solvent phase during the phase inversion process [14].

The efficacy of the membrane was assessed using a cross flow testing apparatus with an active membrane surface area of 20 cm^2 at 20°C (Fig. 1). Initially, deionized water was used to compress all membranes at 0.15 MPa for duration of 30 min. Thereafter, the pressure was reduced to 0.1 MPa, and the flux of pure water was documented at five-minute intervals, with the initial water flux monitored for one hour. The permeate flux (J) was then calculated using Eq. (3).

$$J = \frac{V}{At}, \quad (3)$$

where J is the permeation flux [L/(m^2 h)], V is the permeate volume (L), A is the effective membrane area (m^2), and t is time (hour). To assess the performance of nanocomposite membranes, a 3 ppm MB solution was used as the feed under 1 bar of filtration pressure. The concentrations of the MB solution were determined by measuring the absorbance of MB with a UV-vis spectrophotometer at a wavelength of 663 nm. The MB rejection was subsequently computed based on the difference between the feed and permeate concentration, as per Eq. (4) [15].

$$R(\%) = \left(1 - \frac{C_p}{C_f}\right), \quad (4)$$

where R is the rejection percentage of MB dye (%), C_p is the concentration of the permeate solution (mg/L) and C_f is the concentration of the feed solution (mg/L).

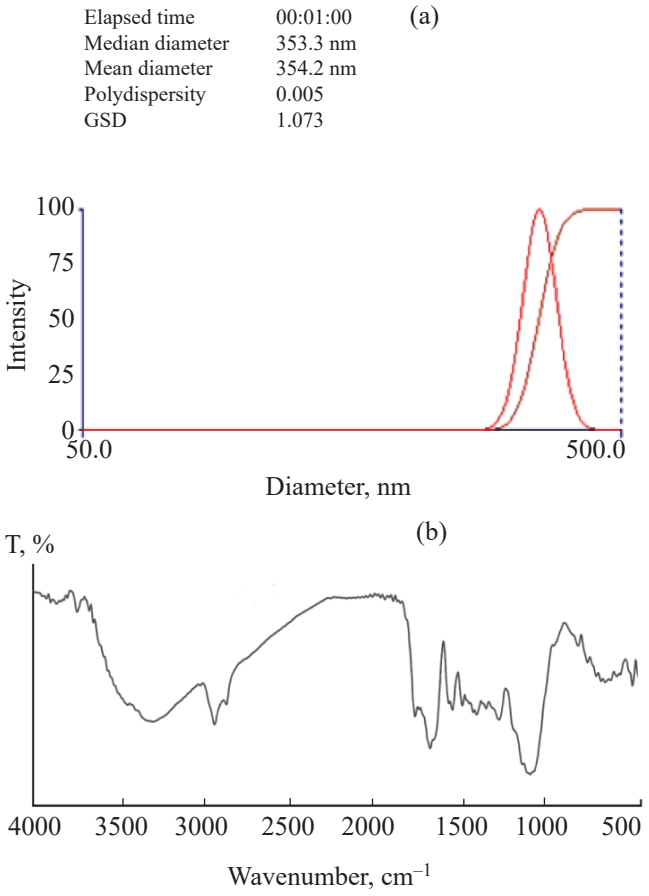

Fig. 2. (a) DLS analysis for average particle size of modified Chm NPs, (b) FTIR spectrum.

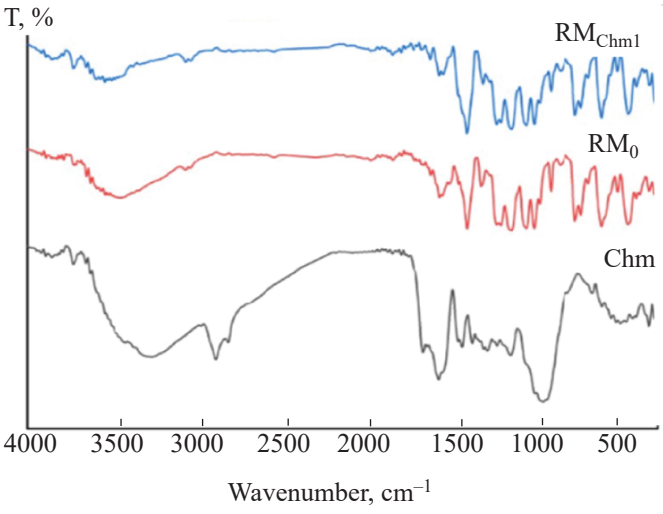

Fig. 3. FTIR spectrum for Chm NPs and the produced PES/Chm membrane.

RESULTS AND DISCUSSION

Characterization of Chm nanoparticle. The dynamic light scattering (DLS) technique allows us to accurately evaluate the size distribution patterns of particles smaller than a micron. Studying the behavior of nanoparticles poses unique challenges and presents distinct opportunities for this approach. The DLS method was utilized to determine the average particle size distribution. As clearly shown in Fig. 2a, the average particle size of the Chm NPs was approximately 353 nm. The functional group of Chm NPs was identified by their FT-IR spectra. A peak at 3420 cm^{-1} was observed in the 3441.9–3470.8 cm^{-1} band, which is associated with the bridging hydroxyl groups in the sample produced, as depicted in Fig. 2b.

Attenuated total reflectance-Fourier transform infrared spectroscopy (ATR-FTIR). The ATR-FTIR spectrum was utilized to showcase the changes in the chemical structure of the membrane's exterior. Fig. 3 displays the FTIR spectra of both the pure PES and PES/Chm membranes. Absorption bands associated with PES were identified for each sample at 1580 cm^{-1}, including the stretching of the benzene ring, a C–C bond at 1490 cm^{-1}, the stretching of aromatic ethers at 1250 cm^{-1}, and a C–O bond at 1100 cm^{-1}. The spectra for the modified membranes differ from that of the unaltered PES membrane. As seen in Chm, hydroxyl (-OH) functional groups can be identified in the spectrum at different wavelengths. The spectrum of the membrane modified with 1 wt % Chm displayed a significant peak at 1680 cm^{-1}, possibly linked to the (C=O) band in the carboxyl group. Moreover, a wide peak was observed in the 3300–3600 cm^{-1} range, suggesting the presence of (OH) groups in the 1 wt % Chm modified membrane. The existence of functional groups, both in the structure and on the surface of the modified PES membranes, is clearly noticeable.

Membrane hydrophilicity. The membrane's hydrophilicity was assessed using water contact angle measurements. Typically, a lower contact angle indicates greater hydrophilicity of the membrane [14]. Figure 4 displays the contact angles (CA) of the PES/Chm membranes containing varying amounts of Chm-NPs (i.e., 0, 0.5, 1, 1.5, and 2 wt %). The CA values diminish from 80.112° for unmodified PES to 47.435° as the amounts of Chm-NPs in the casting solution rise up to 1.5 wt % (Fig. 5). Therefore, we can infer that

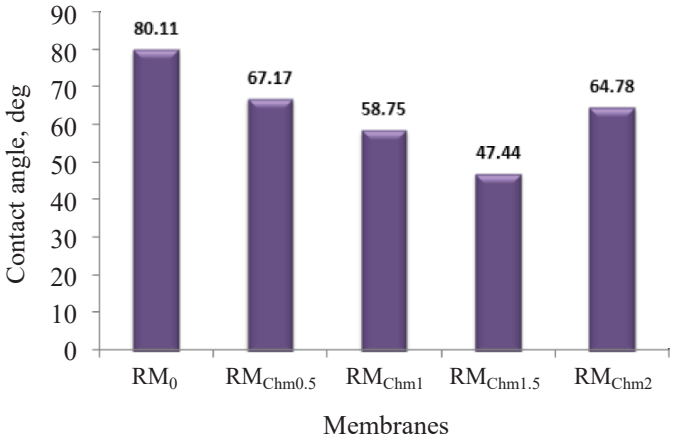

Fig. 4. Contact angle measurements of synthesized membranes.

the inclusion of Chm NPs (up to 1.5 wt %) positively influences the hydrophilicity of the PES/Chm membrane surface, as demonstrated by the approximately 32.67° decrease in the CA value. This reduction could be attributed to the interaction of hydrophilic additive hydroxyl sites with water molecules through hydrogen bonding, which promotes water penetration across the membrane. Conversely, further addition of Chm-NPs led to an elevating CA value reaching 64.78° for 2 wt % Chm-NPs. This is possibly a result of certain factors such as nanoparticle agglomeration in the polymer matrix, diminishing the effects of Chm at high levels in the PES membrane matrix and increasing the contact angle. In addition, similar behavior has been observed in previous studies focusing on membrane surface modification [16, 17].

Morphology of the PES membranes with Rmbedded Chm NPs. The morphology of a membrane plays a critical role in filtration techniques and is influenced by factors such as the interdiffusion rate between solvents and non-solvents, the viscosity of the dope solution, and the coagulation state. This is mainly because, when the casting film encounters a non-solvent in the coagulation bath, a reciprocal diffusion occurs at the interface between the polymer solution and the non-solvent, causing the film to solidify rapidly at that point. Oftentimes, it is the additives that lead to the formation of weak spots on the surface of the solidified polymer. These spots subsequently contribute to the creation of fracture points which, after phase inversion, ultimately transform into pores. The incorporation of Chm dispersion could potentially expedite the demixing process through the enhancement of thermodynamic instability. Moreover, the addition of Chm led to a rise in viscosity of the casting solution, which could potentially decelerate the demixing rate. Throughout the phase separation process, apart from those particles that chemisorb on the surface, the Chm dispersion would be partially leached out from the casting film, serving as a factor in pore formation. This result is in line with a similar finding reported in previous studies [18–20].

As depicted in Fig. 6, all the manufactured membranes possess a uniquely asymmetric cross-sectional structure. This architecture comprises a distinctive blend of finger-like and sponge-like pore structures in the sub-layer, along with a sponge-like pore construct in the selective thin upper layer. Augmenting the amount of Chm influences the entire cross-sectional design of the

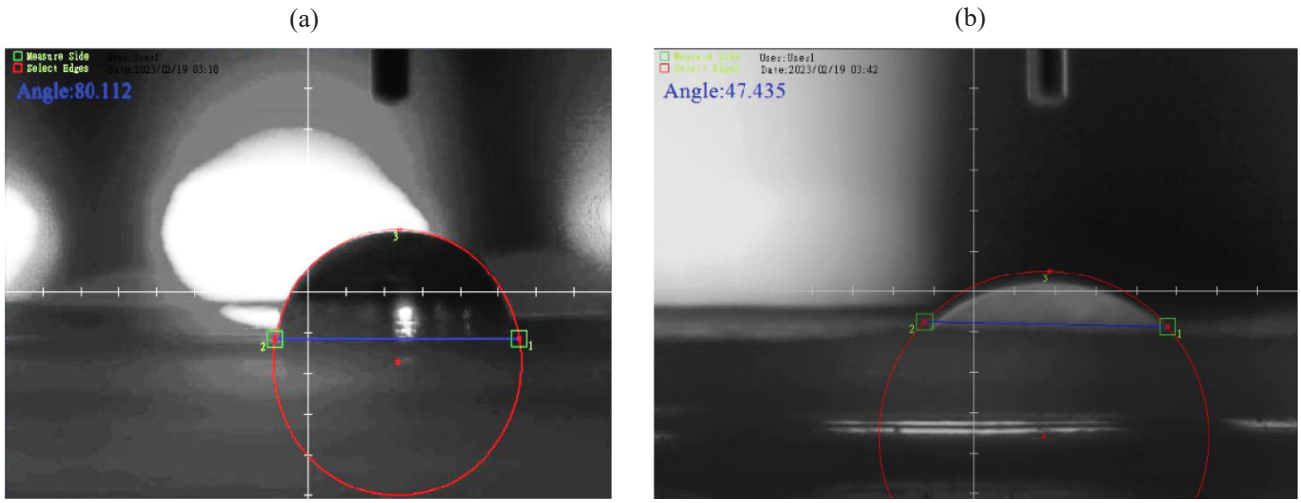

Fig. 5. Images (a) RM_0, (b) $RM_{Chm1.5}$ contact angle PES membrane.

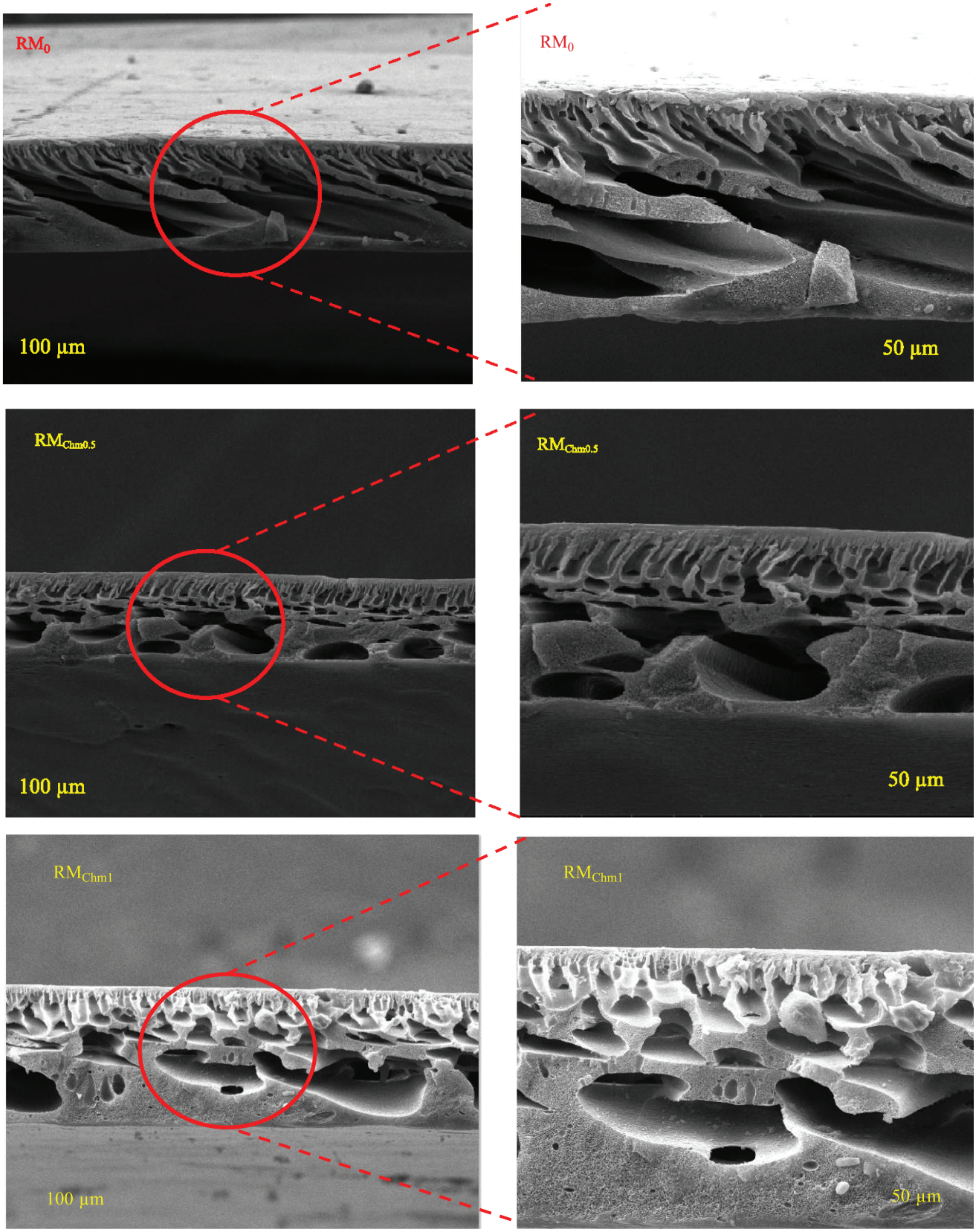

Fig. 6. Cross-sectional FE-SEM images of the PES/Chm membranes.

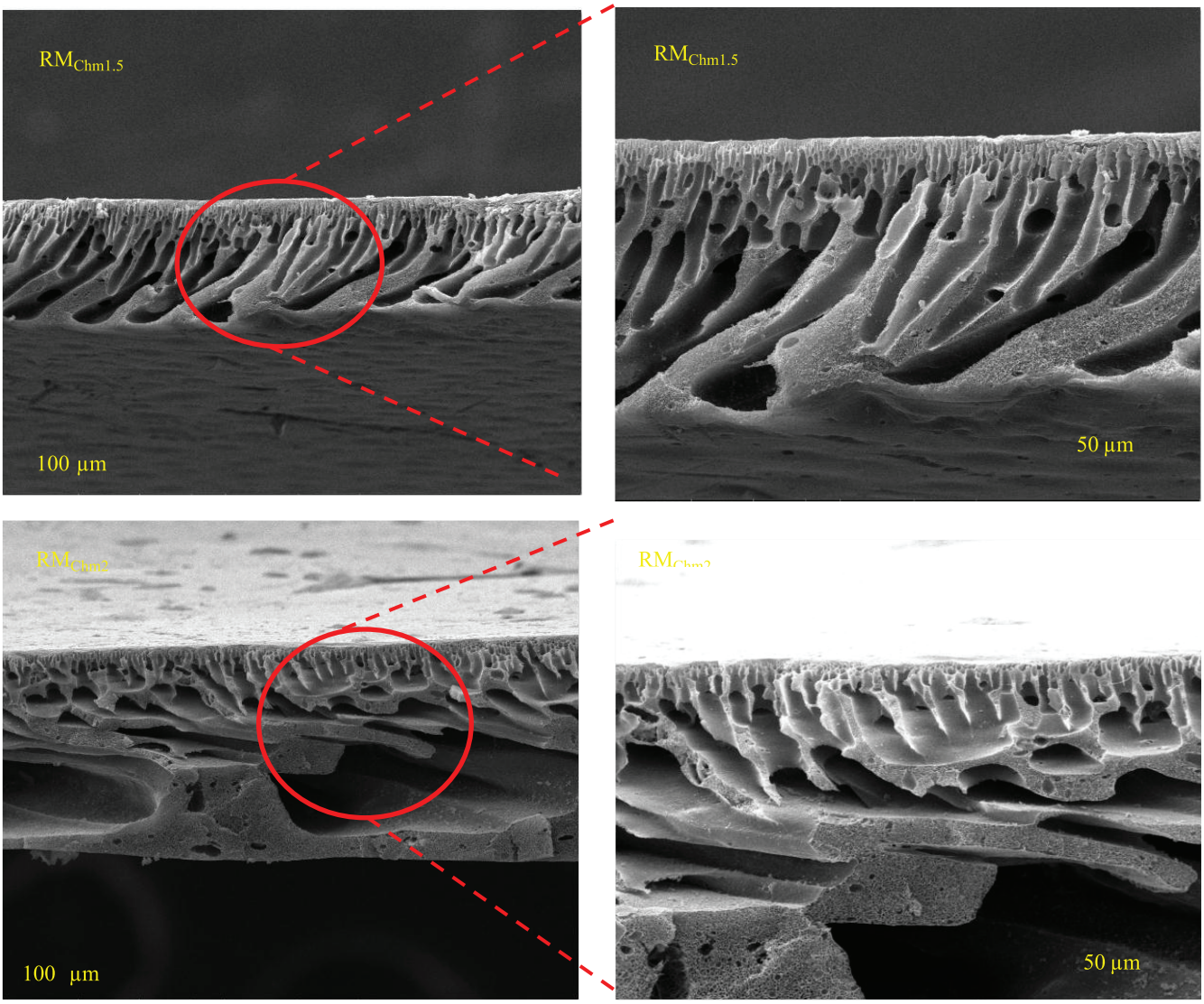

Fig. 6. (Contd.).

membrane, leading to the formation of elongated finger-like structures (as demonstrated in Fig. 6). Furthermore, the sizeable gap in the membrane's sublayer gets filled, facilitating a more porous structure in the sublayer [21].

The FE-SEM images also indicate that membranes, created by incorporating a lower amount of Chm into the dope solution, demonstrated considerable voids within the sub-layer. As a result, compared to a pure PES membrane, the addition of a small quantity of Chm to the casting solution resulted in a more porous sub-layer, featuring larger finger-like pores and thinner pore wall thickness. Furthermore, the thickness of the dense skin layer noticeably reduced when the Chm concentration was increased to 1.5 wt %. Possible reasons behind this occurrence could be twofold, specifically Firstly, the alterations in the membrane structures due to the introduction of Chm can be comprehended in reference to the membrane formation mechanism during phase separation. The integration of Chm caused the miscibility of the casting solution with water to diminish, hence hastening the phase separation process. When the casting film came into contact with the nonsolvent in the coagulation bath, there was a swift withdrawal of the solvent from the casting film into the bath, causing the diffusive migration of soluble additives. As a result, some Chm was removed from the casting film along with the NMP. This enabled it to function as an agent for pore formation during the membrane creation process, leading to increased porosity and enlargement of the surface pores on the membrane.

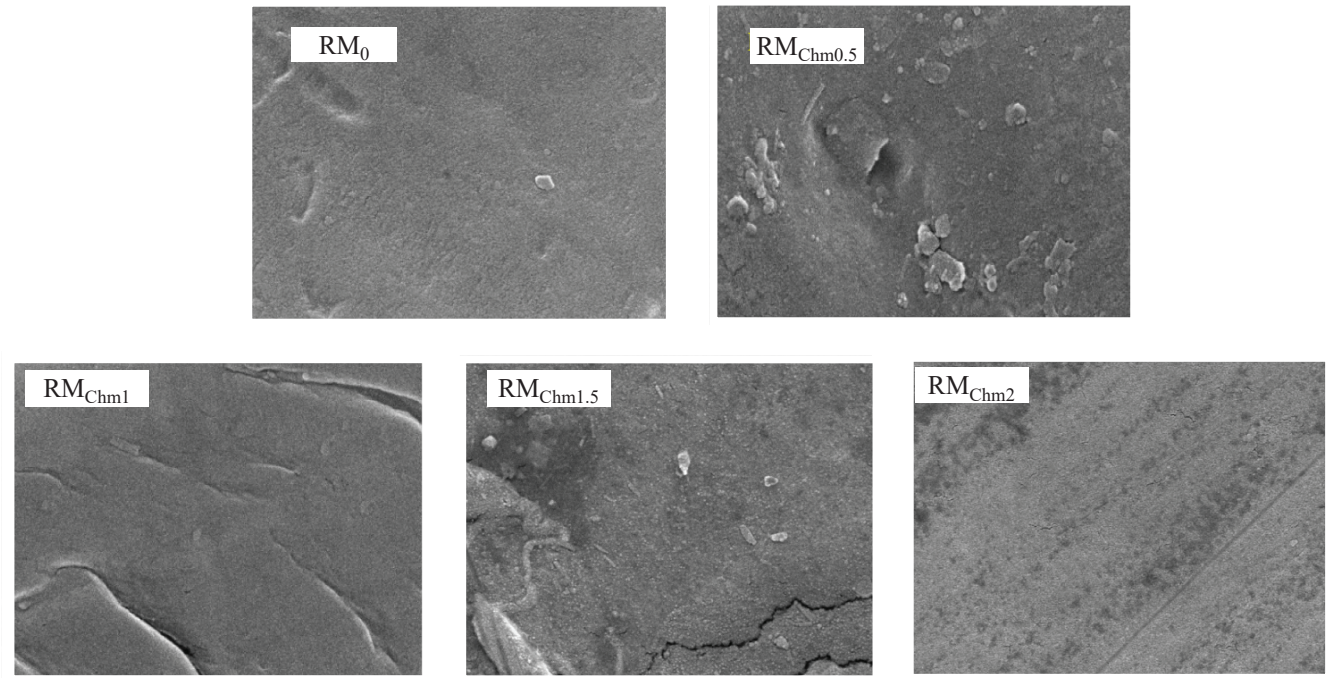

Fig. 7. Top surface FE-SEM photographs of the PES/Chm membranes.

Moreover, the existence of hydroxyl groups attached to Chm in the dope solution enhances the exchange speed between the non-solvent and the solvent during the phase inversion process. This results in the creation of more elaborate finger-like structures. It is noteworthy that when the Chm concentration reached 2 wt % in the casting solution, the thickness of the pore wall increased and the membrane porosity reduced due to an increase in viscosity of the dope solution linked to the rise of Chm concentration (greater than 2 wt % in the dope solution). Because of this high viscosity, the amount of Chm diffusing out of the casting film significantly reduced, thereby diminishing the Chm's pore-forming effect. In addition, the elevated viscosity of the casting solutions obstructed the creation and expansion of membrane pores, leading to a reduction in the membrane's porosity and surface pore size. This finding is consistent with observations reported in previous studies [22–24].

Figure 7 presents images of the top surface of the pure PES membrane as well as the modified PES/Chm membrane. With the addition of Chm nanoparticles to the PES polymer matrix, it was evident that the surface of the pure PES membrane (the RM PES membrane) displayed a smooth, nodule-free surface. Moreover, the surface pore structure was completely transformed, exhibiting smaller pores after this adjustment. The introduction of Chm at a concentration of 0.5 wt % led to the noticeable formation of pores on the membrane surface (RM_{Chm1}). The distribution of Chm nanoparticles showed homogeneity at both low and high concentrations even though minor clusters were present. This can be attributed to the improved hydrophilicity of the Chm nanoparticles stemming from their synergistic properties. Additionally, embedding nanoparticles diminishes the interaction between the polymer and solvent. Therefore, the solvent can rapidly migrate from the pristine membrane into the water, resulting in a quicker rate of liquid-liquid exchange, and ultimately forming a thin, smooth outer skin layer.

Porosity and mean pore size measurement. Analyzing pore size and membrane porosity is crucial; as they directly impact the membrane's rejection ability and permeation flux, respectively. Typically, the porosity of a membrane is tied to the mass transfer rate between the solvent and non-solvent phase during the phase inversion process [14]. Figure 8 indicates an increase in membrane porosity for the versions of the membrane with RM Chm loading (0.5, 1 and 1.5 wt %), compared to the MR_0 membrane, as calculated by Eq. (2). The different membranes' porosities ranged

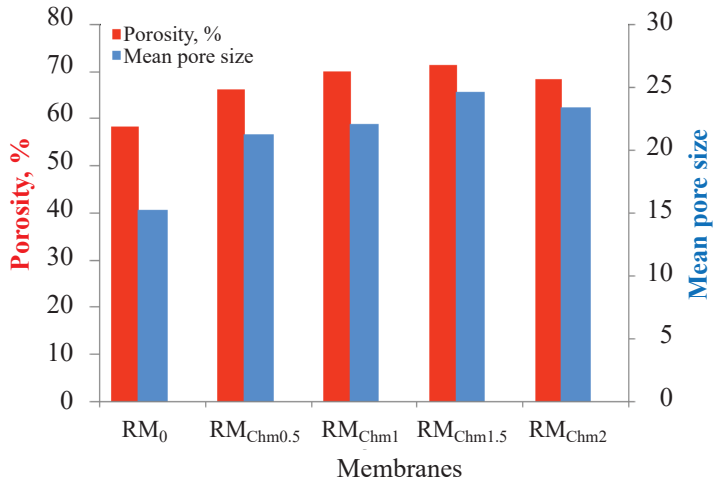

Fig. 8. Influence of Chm concentration on the porosity and mean pore diameter of the PES membrane.

considerably from 58.3 to 71.5%. The lowest porosity, 58.3%, was observed for the pristine membrane. After the incorporation of 0.5 wt % of Chm, porosity increased to 67.2%. Continuing this upward trend, with the addition of 1.5%, porosity reached a peak of 71.5%. This increase suggests that the rapid exchange of solvent and nonsolvent during the phase inversion process could be triggered by hydrophilic additives in the polymer matrix, consequently improving the formation of pores in the prepared membrane [25]. As a result, the porosity of these membranes was augmented. While still greater than the porosity of a pure membrane, it is crucial to point out that with a Chm nanoparticle loading ratio above this, the porosity decreased to 68.8% when 2 wt % of the dope was incorporated. It was speculated that with a 2 wt % Chm nanoparticle loading, the high viscosity of the casting solution could exceed the hydrophilicity influence of the Chm nanoparticles, resulting in a reduced mass transfer rate between the solvent and nonsolvent phase during the phase inversion process. This decrease in mass transfer rate could, in turn, lead to a decrease in pore formation at high Chm nanoparticle loading.

On the other hand, the mean pore radius, another crucial surface parameter, significantly influences the performance of the membrane. As seen in Fig. 8, the creation of highly porous membranes was evidently aided by integrating Chm nanoparticles into the polymeric solution. The formulation of larger pores during the separation phase was facilitated by the addition of Chm nanoparticles, acting as a water-soluble pore generator. This addition led to a slower solvent exchange rate, thus creating bigger pores. A membrane made with 0.5 wt % of Chm nanoparticles exhibited a considerably larger mean pore radius compared to the plain membrane, which had a mean pore radius of 15.2 nm. With the addition of 1.5 wt % Chm nanoparticles, a larger mean pore radius of 24.6 nm was noticed. Importantly, a slight reduction in the pore radius was recorded when raising the Chm concentration to 2 wt % in the polymeric matrix. Likely due to particle build-up, this led to a narrowed or blocked membrane pores diameter due to high loading aggregation of Chm nanoparticles [1]. Furthermore, augmenting the quantity of nanoparticles in the membrane solution resulted in an enhanced viscosity of the solution. This, in turn, caused a decrease in both the pore size and the porosity of the membranes.

Membrane thickness. Both the modified and unmodified PES membranes showcased a thickness close to 120 μm, considered ideal for the ultrafiltration membrane process for wastewater separation, as per prior research. As shown in Fig. 8, the membrane thickness grew from 98.77 μm for a plain PES membrane to 105.34 μm upon introducing 0.5 wt % Chm nanoparticles, highlighting the thickness of both PES neat and PES/Chm nanoparticles. The membrane thickness continued to escalate as the Chm additive concentration increased, reaching up to 172 μm at 2 wt % of Chm, as show in Fig. 9. This may be attributed to the viscosity increase of the casting solution due to the heightened concentration of Chm nanoparticles. Reports suggest that the augmentation in membrane thickness was triggered by the heightened amount of nanomaterial components in the casting solution, as stated in reference [26].

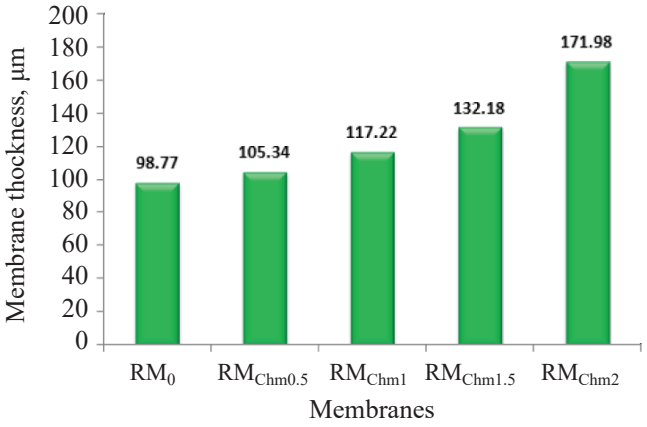

Fig. 9. Influence of Chm concentration on thickness of the PES membranes.

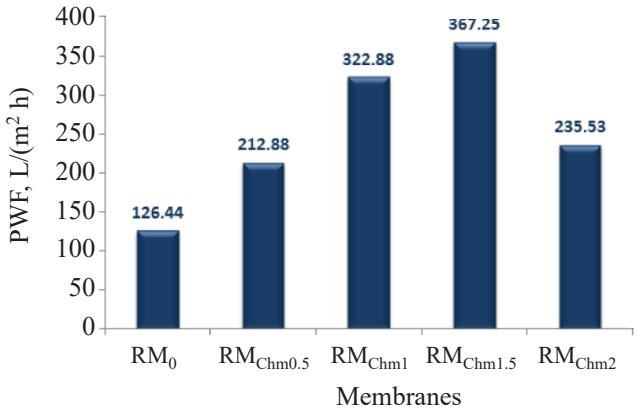

Fig. 10. Effects of Chm NPs/PES membranes on Pure Water Flux.

MEMBRANE PERFORMANCE EVALUATION

Membrane pure water permeability. Cross-flow ultrafiltration experiments were conducted to assess the separation capabilities of the fabricated PES membranes. Fig. 10. displays the pure water flux (PWF) of the prepared membranes. The PWF of the PES membranes, modified with hydrophilic Chm additions, was found to exceed that of the unmodified PES membranes. The water flux noted a significant increase as the additive content rose from 0.5 to 1.5 wt %. With just 0.5 wt % Chm added to the dope solution, the pure water flux ascended to 212.879 L/(m^2 h), in contrast to the 126.442 L/(m^2 h) for the unadulterated membrane. The $RM_{Chm1.5}$ (1.5 wt % Chm NPs) reported a significantly higher PWP of 367.25 L/(m^2 h) when compared with the RM0 membrane. This could be due to the possibility that an increase in Chm NPs in the casting solution could accelerate the diffusion rate of solvents and non-solvents in the coagulation bath, resulting in swifter precipitation and the formation of a finger-like structure, as supported by the FE-SEM analysis (Fig. 6). Consequently, the membranes' resistance could be minimized, leading to enhanced water permeability performance. This could be explained by the increment in membrane porosity that in turn led to a higher pure water flow. Other plausible reasons could include an increase in average pore size [27]. Moreover, an increase in the amount of Chm nanoparticles induced by the incorporation of (–OH) groups conjugated with the nanoparticle structure might enhance the water absorption capacity of the membrane, allowing more water molecules to pass, thus delivering a higher membrane flux [28]. Nevertheless, increasing the Chm content to 2 wt % led to decline in PWP for the RM_{Chm2} membrane, settling at 235.53 L/(m^2 h). This could be attributed to a decrease in membrane porosity, pore size and membrane hydrophilicity [29].

Permeability and rejection of Methylene Blue (MB). Methylene Blue (MB) is a basic dye recognized for its aromatic heterocyclic characteristics. It possesses a molecular weight of 319.85 g mol^{-1} and is prominently water-soluble, forming a stable solution at room temperature. As a part of the polymethine dye class, MB contains an amino autochrome unit, behaving as a positive compound. However, MB dye can be significantly toxic when its concentration exceeds certain levels. Due to its toxicity, carcinogenic nature, and resistance to biodegradation, MB presents serious risks to both human health and the environment. Given these concerns, it becomes essential to remove MB [30, 31]. Membrane technology has emerged as one of the most suitable methods for this purpose, as it has demonstrated noteworthy efficiency in the past couple of decades. Figures 11, 12 illustrate the influence of Chm NPs as eco-friendly additives on the rejection behavior and permeability of the modified membranes in our investigation, the rejection capabilities of the modified membranes at defined 0.5, 1, 1.5 wt % Chm NPs were (86.27, 93.58, 88.81%, respectively. Notably, these are quite efficient compared to the unmodified membrane. The rejection procedure relies on two fundamental factors: the size of pores dispersed on the membrane surface and the electrostatic interaction between the dye and the membrane. The additive, spread across the membrane's surface, functioned as an absorbing surface, capturing the dye upon contact. Notably, an increase in the additive's weight percentage

resulted in a reduced dye rejection. The most effective membrane for dye rejection was RM_{Chm1} with a rejection ratio of 93.58% (Fig. 13). Additionally, the flux of the MB dye consistently increased at Chm NPs concentrations of 0.5, 1, and 1.5 wt %, reaching a maximum flux of 281 L/(m^2 h) at 1.5 wt % Chm NPs. However, when the Chm NPs concentration was increased to 2%, there was a noted decline in flux.

PROPOSED INTERACTION MECHANISMS

The addition of Chm has been demonstrated to enhance the permeability, selectivity, and antifouling properties of modified membranes. This enhanced interaction between the PES and Chm series may be accountable for the improved surface features of the modified membranes. According to research findings, the interaction mechanisms involving PES and Chm membranes modify their relationship with water molecules, which is portrayed in Fig. 14.

The inclusion of flexible hydrophilic functional groups could potentially explain the enhanced compatibility between the Chm and PES chains, which in turn influences the fluctuating surface characteristics of PES mixed matrix membranes (MMMs). The interactions formed between the membrane surface and water molecules are directly attributable to this. The presence of these functional groups facilitates the easier establishment of hydrogen bonds between water molecules, forming a wetting layer on the membrane surface. All these factors collectively enhance the membrane's wettability and permeability, thereby elevating the overall system efficiency. Besides, the fact that electronegative atoms like oxygen are present boosts the likelihood of forming hydrogen bonds. Oxygen's high electronegativity means it attracts more of its bond's electron density away from hydrogen, creating a partially positive H that is highly electron-deficient, stabilizing the bonds formed with oxygen. Hydrogen bonding with oxygen results in a confined space capable of holding water, effectively increasing the hydrophilicity of the MMM. As depicted in the figure, for the PES/Chm membrane, an OH bond between Chm and PES along with a hydrogen bond between the bound groups and the water molecule is typically anticipated.

Initially, hydrogen bonds form with the polymer's oxygen. As the proportion of Chm introduced to the polymer rises, so does the opportunity for forming hydrogen bonds, up until saturation is achieved. This presents additional hydrophilic sites, specifically the

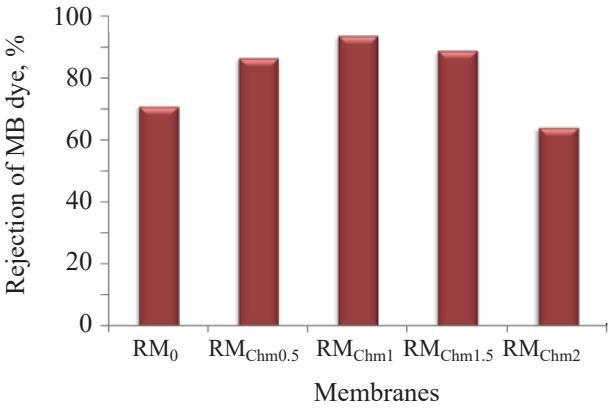

Fig. 11. Effect of Chm NPs on methylene blue (MB) rejection, %.

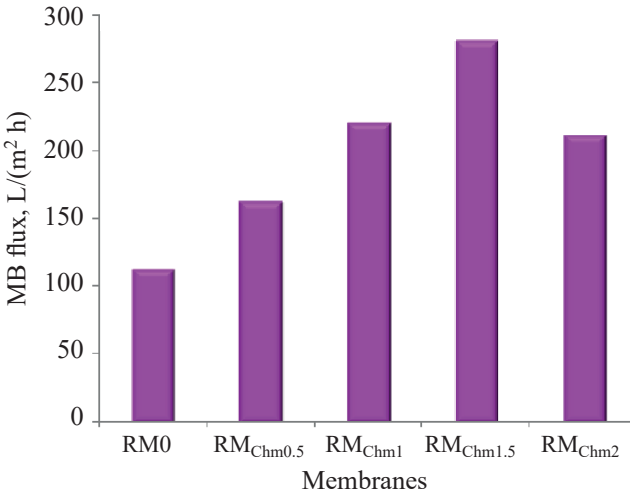

Fig. 12. Effect of Chm NPs on methylene blue (MB) flux.

hydroxyl groups in the Chm, which subsequently form hydrogen bonds with water during casting. This leads to the highest percentage of hydrophilicity and the largest pore diameters. However, when the quantity of additives is increased further, hydrophilicity reduces due to the diminished solubility of Chm in water, as its solubility is relatively low. Manufacturers recommend a solubility percentage of between 0.5 and 2 wt %. As a result, this increased additive percentage gives rise to greater thickness, but fewer pores.

Comparing the present study with previous research. Table 2 provides a summary of the strategies employed for membrane modification. A comparative analysis can be made between the characteristics and performance of PES membranes synthesized in this study and those selected from existing literature. Key attributes, like hydrophilicity of the membranes, have

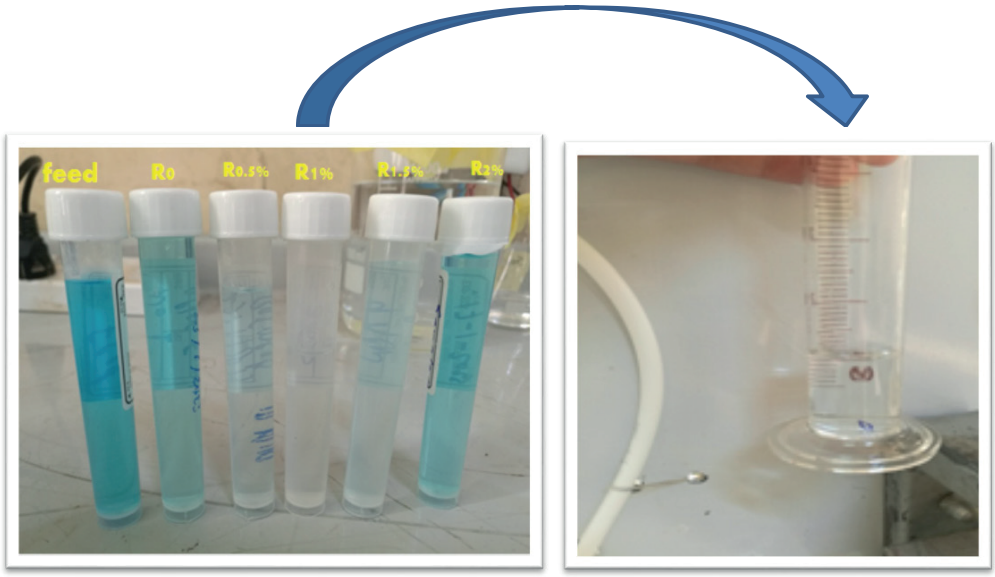

Fig. 13. Images show the rejection of methylene blue in membrane modification with Chm NPs.

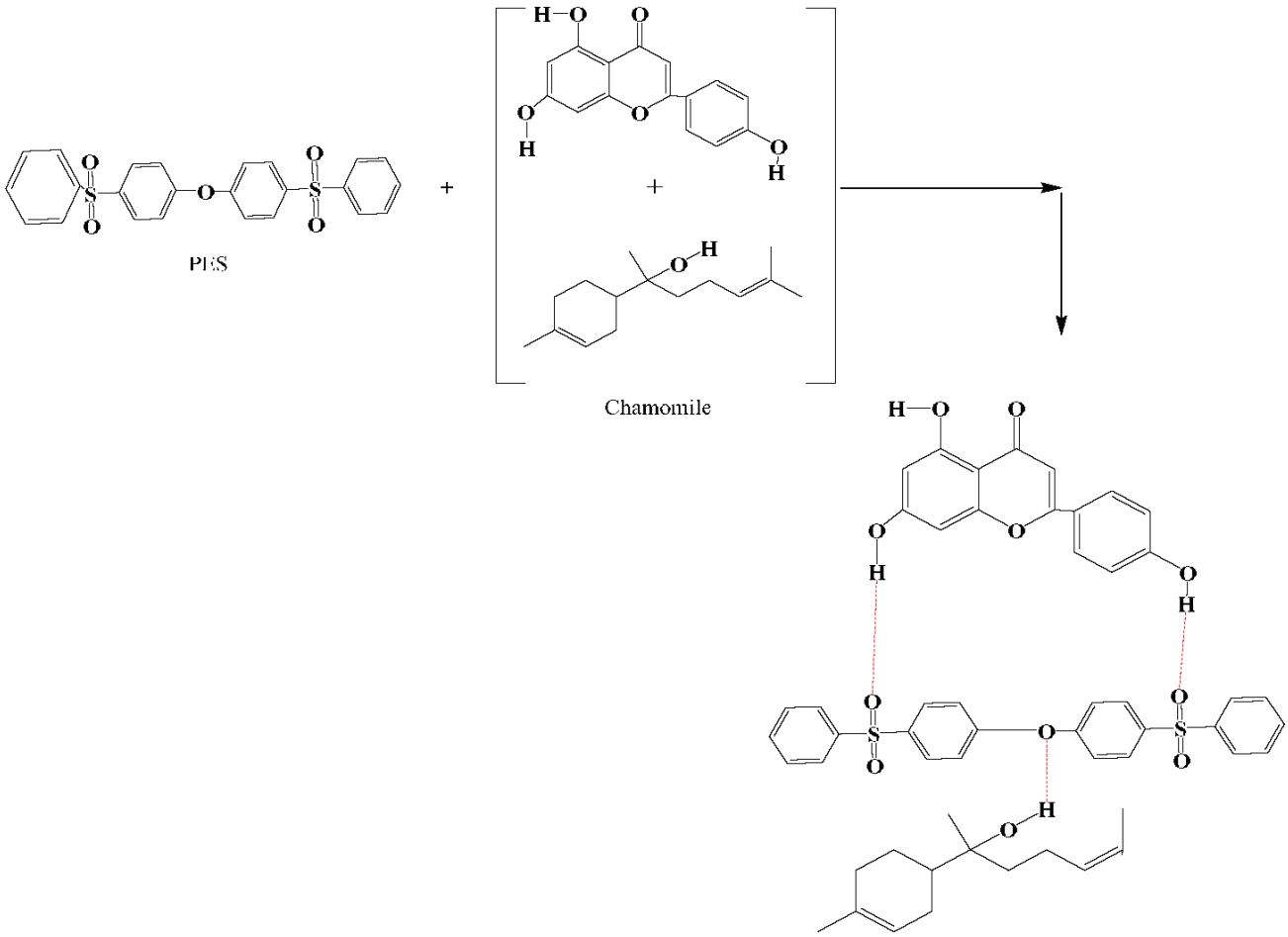

Fig. 14. Proposed mechanisms of interaction between PES/Chm membrane components and water molecules.

Table 2. A comparison between the findings of our study and those selected from recent literature

Base material	Modifier NPs	Contact angle, deg	Porosity, %	Mean pore size, nm	Flux, L/(m^2 h)	Rejection	Ref.
PPSU + NMF	Gum arabic graphene (GGA)	49		95.57	82.11	88% Sodium alginate	[20]
Polysulfone (PSf)	Graphene oxide (GO) + gum arabic	55.47	78.37	20.76	58.68 at 4 bar	99.67% Humic acid (HA)	[10]
Polyamide 6.6 + formic acid	Silver-graphene oxide (Ag-GO)	39.4	More than 80	8.2	NA	Higher than 95% for both BSA and Congo Red	[15]
PVC	Gum arabic	65.1	66.3	33	93	96% HA	[32]
Polysulfone (PSf)	Iron oxide-decorated grapbene oxide (Fe_3O_4/GO)	69.97	76.35	34.7	112.47	97%	[13]
PVC	Clay nanopartides (CNs)	63.3	89.67	8.4	40.72	94.78%	[33]
PES-PVP + DMAC	SiO_2	59.5	75		19.40	92.1% Rhodamiue B (RbB) dye	[34]
PES + PVP + DMAc	Goethite-tannic acid	63.43	75	5.5	NA	92.6% Direct-Red 16.4 bar	[35]
Poly(ether ether sulfone) (PEES) + NMP	*n*-ZnQ	49.69	28.7	6.43	166.73	98.03% HA	[35]
PES-NMP	Chamomile NPs (Chm)	47.44	71.5	24.6	280.822	93.58% MB dye	Current study

been highlighted. When compared to other membranes selected from outside sources, the performance of these membranes seems to hold appreciable merit.

CONCLUSIONS

(1) In order to fabricate a hydrophilic ultrafiltration membrane, Chm NPs were prepared and incorporated into PES polymer casting solution.

(2) FTIR research revealed functional groups on the surface of Chm NPs. The hydrophilicity of the membranes increased substantially with increasing nanoparticle concentration, as determined by the water contact angle measurements,, and the water transport through the modified membrane was considerably enhanced.

(3) As Chm NPs content increased, the cross-sectional morphologies noticeably changed from finger-like to microporous and then to dense structures.

(4) A marginally elevated surface topography and smaller mean pore size were observed. The membrane's porosity, mean pore size, and contact angle were all improved by the addition of Chm NPs.

(5) The evaluation of the membranes' ultrafiltration performance with respect to the removal of MB dye revealed that the introduction of O–H with Chm NPs nanoparticles resulted in the induction of surface features on the membrane and an increase in dye rejection.

(6) The filtration results are promising and suggest that the prepared Chm NPs ultrafiltration membrane may be beneficial for wastewater treatment efforts in the textile industry.

AUTHOR INFORMATION

Rana I. Raja, ORCID: https://orcid.org/0009-0001-0517-6780

Khalid T. Rashid, ORCID: https://orcid.org/0000-0001-7794-5174;

Manal A. Toma, ORCID: https://orcid.org/0000-0001-5692-5633FUNDING.

FUNDING

This work was supported by ongoing institutional funding. No additional grants to carry out or direct this particular research were obtained.

CONFLICT OF INTEREST

The authors declare that they have no conflict of interest.

REFERENCES

1. Mu, Y., Zhu, K., Luan, J., Zhang, S., Zhang, C., Na, R., Yang, Y., Zhang, X., and Wang, G., *Journal of Membrane Science,* 2019, vol. 577, pp. 274–284. https://doi.org/10.1016/j.memsci.2019.01.043
2. Datta, S., Karmoker, S., and Sowgath, M.T., *Conference, Environmental Division,* 2012.
3. Vinh-Thang, H. and Kaliaguine, S., *Chemical Reviews,* 2013, vol. 113, pp. 4980–5028. https://doi.org/10.1021/cr3003888
4. Shihab, J.M., Toma, M.A., Hussein, A.D., and Rashid, K.T., *Chemistry Africa,* 2024, vol. 7, pp. 281–290. https://doi.org/10.1007/s42250-023-00757-6
5. Foong, Y.X., Yew, L.H., and Chai, P.V., *Materials Today: Proceedings,* 2021, vol. 46, part 5, pp. 2092–2097. https://doi.org/10.1016/j.matpr.2021.04.470.
6. Rodrigues, R., Mierzwa, J.C., and Vecitis, C.D., *Journal of Water Process Engineering,* 2019, vol. 31, ID 100788. https://doi.org/10.1016/j.jwpe.2019.100788
7. Ahmadi, H., Jahanshahi, M., Peyravi, M., and Darzi, G.N., *Journal of Cleaner Production*, 2022, vol. 334, ID 130114. https://doi.org/10.1016/j.jclepro.2021.130114
8. Saja, S., Bouazizi, A., Achiou, B., Ouaddari, H., Karim, A., Ouammou, M., Aaddane, A., Bennazha, J., and Alami Younssi, S., *Journal of the European Ceramic Society,* 2020, vol. 40, no. 6, pp. 2453–2462. https://doi.org/10.1016/j.jeurceramsoc.2020.01.057
9. Manawi, Y., Kochkodan, V., Mohammad, A.W., and Atieh, M.A., *Journal of Membrane Science,* 2017, vol. 529, pp. 95–104. https://doi.org/10.1016/j.memsci.2017.02.002
10. Chai, P.V., Choy, P.Y., Teoh, W.C., Mahmoudi, E., and Ang, W.L., *Journal of Environmental Chemical Engineering,* 2021, vol. 9, no. 4, ID 105638. https://doi.org/10.1016/j.jece.2021.105638
11. Marjani, A., Nakhjiri, A.T., Adimi, M., Jirandehi, H.F., and Shirazian, S., *Scientific Reports,* 2020, vol. 10, no. 1, ID 2049. https://doi.org/10.1038/s41598-020-58472-y
12. Rahimpour, A., Madaeni, S.S., and Mansourpanah, Y., *Desalination,* 2010, vol. 258, nos. 1–3, pp. 79–86. https://doi.org/10.1016/j.desal.2010.03.042
13. Chai, P.V., Mahmoudi, E., Mohammad, A.W., and Choy, P.Y., *IOP Conf. Ser.: Earth Env. Sci.,* 2020, vol. 463, no. 1, ID 012174. https://doi.org/10.1088/1755-1315/463/1/012174
14. Chai, P.V., Law, J.Y., Mahmoudi, E., and Mohammad, A.W., *Journal of Water Process Engineering,* 2020, vol. 38, ID. 101673. https://doi.org/10.1016/j.jwpe.2020.101673
15. Naji, M.A., Salimi-Kenari, H., Alsalhy, Q.F., Al-Juboori, R.A., Huynh, N., Rashid, K.T., and Salih, I.K., *Membranes,* 2023, vol.13, no. 3, ID 357. https://doi.org/10.3390/membranes13030357
16. Homem, N.C., Beluci, N.D.C.L., Amorim, S., Reis, R., Vieira, A.M.S., Vieira, M.F., Bergamasco, R., and Amorim, M.T.P., *Applied Surface Science,* 2019, vol. 486, pp. 499–507. https://doi.org/10.1016/j.apsusc.2019.04.276
17. Zinadini, S., Zinatizadeh, A.A., Rahimi, M., Vatanpour, V., and Zangeneh, H., Journal of *Membrane Science,* 2014, vol. 453, pp. 292–301. https://doi.org/10.1016/j.memsci.2013.10.070
18. Shukla, A.K., Alam, J., Alhoshan, M., Dass, L.A., and Muthumareeswaran, M.R., *Scientific Reports,* 2017, vol. 7, no. 1, ID 41976. https://doi.org/10.1038/srep41976
19. Mahmoudi, E., Ng, L.Y., Ang, W.L., Chung, Y.T., Rohani, R., and Mohammad, A.W., *Scientific Reports,* 2019, vol. 9, no. 1, ID 1216. https://doi.org/10.1038/s41598-018-38060-x
20. Ali, A.M., Rashid, K.T., Yahya, A.A., Majdi, H.S., Salih, I.K., Yusoh, K., Alsalhy, Q.F., AbdulRazak, A.A., and Figoli, A., *Membranes,* 2021, vol. 11, no.7, ID 542. https://doi.org/10.3390/membranes11070542
21. Emadzadeh, D., Lau, W.J., Matsuura, T., Rahbari-Sisakht, M., and Ismail, A.F., *Chemical Engineering Journal,* 2014, vol. 237, pp. 70–80. https://doi.org/10.1016/j.cej.2013.09.081
22. Zhao, S., Wang, Z., Wei, X., Zhao, B., Wang, J., Yang, S.,

and Wang, S., *Journal of Membrane Science,* 2011, vol. 385–386, pp. 251–262. https://doi.org/10.1016/j.memsci.2011.10.006

23. Eren, E., Sarihan, A., Eren, B., Gumus, H., and Kocak, F.O., *Journal of Membrane Science,* 2015, vol. 475, pp. 1–8. https://doi.org/10.1016/j.memsci.2014.10.010
24. Yin, J. and Zhou, J., *Desalination,* 2015, vol. 365, pp. 46–56. https://doi.org/10.1016/j.desal.2015.02.017
25. Yang, Y. and Wang, P., *Polymer,* 2006, vol. 47, no. 8, pp. 2683–2688. https://doi.org/10.1016/j.polymer.2006.01.019
26. Urkiaga, A., Iturbe, D., and Etxebarria, J., *Desalination and Water Treatment,* 2015, vol. 56, no. 13, pp. 3415–3426. https://doi.org/10.1080/19443994.2014.1000976
27. Vatanpour, V., Dehqan, A., and Harifi-Mood, A.R., *Journal of Membrane Science,* 2020, vol. 614, ID 118528. https://doi.org/10.1016/j.memsci.2020.118528
28. Mulyati, S., Muchtar, S., Yusuf, M., Arahman, N., Sofyana, S., Rosnelly, C.M., Fathanah, U., Takagi, R., Matsuyama, H., Shamsuddin, N., and Bilad, M.R., *Membranes,* 2020, vol. 10, no. 1, ID 17. https://doi.org/10.3390/membranes10010017
29. Sabri, S., Najjar, A., Manawi, Y., Eltai, N.O., Al-Thani, A., Atieh, M.A., and Kochkodan, V., *Membranes,* 2019, vol. 9, no.2, ID 29. https://doi.org/10.3390/membranes9020029
30. Khan, I., Saeed, K., Zekker, I., Zhang, B., Hendi, A.H., Ahmad, A., Ahmad, S., Zada, N., Ahmad, H., Shah, L.A. Shah, T., and Khan, I., *Water,* 2022, vol. 14, no. 2, ID 242. https://doi.org/10.3390/w14020242
31. Sun, L., Hu, D., Zhang, Z., and Deng, X., *International Journal of Environmental Research and Public Health,* 2019, vol. 16, no. 23, ID 4773. https://doi.org/10.3390/ijerph16234773
32. Aji, M.M., Narendren, S., Purkait, M.K., and Katiyar, V., *Journal of Water Process Engineering,* 2020, vol. 38, ID 101569. https://doi.org/10.1016/j.jwpe.2020.101569
33. Ferdowsi, A., Kikhavani, T., and Ashrafizadeh, S.N., *Enhancement in Performance of the PVC/Nanoclay Mixed Matrix Nanofiltration Membrane,* 2022. https://doi.org/10.21203/rs.3.rs-1741723/v1
34. Otitoju, T.A., Ahmadipour, M., Li, S., Shoparwe, N.F., Jie, L.X., and Owolabi, A.L., *Journal of Water Process Engineering,* 2020, vol. 36, ID 101356. https://doi.org/10.1016/j.jwpe.2020.101356
35. Saniei, N., Ghasemi, N., Zinatizadeh, A.A., Zinadini, S., Ramezani, M., and Derakhshan, A.A., *Separation and Purification Technology,* 2020, vol. 241, ID 116646. https://doi.org/10.1016/j.seppur.2020.116646
36. Purushothaman, M., Arvind, V., Saikia, K., and Vaidyanathan, V.K., *Chemosphere,* 2022, vol. 286, ID 131616. https://doi.org/10.1016/j.chemosphere.2021.131616